Pre-print

Malusà, M. G., Wang, J., Garzanti, E., Liu, Z. C., Villa, I. M., & Wittmann, H. (2017).

Trace-element and Nd-isotope systematics in detrital apatite of the Po river catchment: Implications for provenance discrimination and the lag-time approach to detrital thermochronology.

Lithos, 290, 48-59.

http://dx.doi.org/10.1016/j.lithos.2017.08.006

Trace-element and Nd-isotope systematics in detrital apatite of the Po river catchment: implications for provenance discrimination and the lag-time approach to detrital thermochronology

Marco G. Malusà[1]*, Jiangang Wang[2*], Eduardo Garzanti[1],
Zhi-Chao Liu[2,3], Igor M. Villa[1,4], Hella Wittmann[5]

[1]Department of Earth and Environmental Sciences, University of Milano-Bicocca, Milano, Italy
[2]Institute of Geology and Geophysics, Chinese Academy of Sciences, Beijing, China
[3]Sun Yat-Sen University, Guangzhou, China
[4]Institute of Geological Sciences, University of Bern, Switzerland
[5]GFZ German Research Centre for Geosciences, Potsdam, Germany

*Corresponding author. Tel.:+39 02 6448 2065; fax: +39 02 6448 2073.
E-mail addresses: marco.malusa@unimib.it (Marco Giovanni Malusà); wangjiangang@mail.iggcas.ac.cn (Jiangang Wang)

Abstract

Detrital thermochronology is often employed to assess the evolutionary stage of an entire orogenic belt using the lag-time approach, i.e, the difference between the cooling and depositional ages of detrital mineral grains preserved in a stratigraphic succession. The impact of different eroding sources to the final sediment sink is controlled by several factors, including the short-term erosion rate and the mineral fertility of eroded bedrock. Here, we use apatite fertility data and cosmogenic-derived erosion rates in the Po river catchment (Alps-Apennines) to calculate the expected percentage of apatite grains supplied to the modern Po delta from the major Alpine and Apenninic eroding sources. We test these predictions by using a cutting-edge dataset of trace-element and Nd-isotope signatures on 871 apatite grains from 14 modern sand samples, and we use apatite fission-track data to validate our geochemical approach to provenance discrimination. We found that apatite grains shed from different sources are geochemically distinct. Apatites from the Lepontine dome in the Central Alps show relative HREE enrichment, lower concentrations in Ce and U, and higher $^{147}Sm/^{144}Nd$ ratios compared to apatites derived from the External Massifs. Derived provenance budgets point to a dominant apatite contribution to the Po delta from the high-fertility Lepontine dome, consistent with the range independently predicted from cosmonuclide and mineral-fertility data. Our results demonstrate that the single-mineral record in the final sediment sink can be largely determined by high-fertility source rocks exposed in rapidly eroding areas within the drainage. This implies that the detrital thermochronology record may reflect processes affecting relatively small parts of the orogenic system under consideration. A reliable approach to lag-time analysis would thus benefit from an independent provenance discrimination of dated mineral grains, which may allow to proficiently

reconsider many previous interpretations of detrital thermochronology datasets in terms of orogenic-wide steady state.

Keywords: detrital apatite; mineral fertility; trace elements; Nd isotopes; ^{10}Be-derived erosion rates; lag-time analysis

1. Introduction

Detrital thermochronology is widely employed to investigate the feedback between climate and tectonic activity (Huntington et al., 2006; Wobus et al., 2006; Rahl et al., 2007; Bermúdez et al., 2013), and is often used to infer the evolutionary stage (growing, steady state or decaying) of an entire orogenic belt using the lag-time approach (i.e., the time difference between the cooling age and the depositional age of a detrital mineral grain; Garver et al., 1999). The fingerprint of modern river sediments provides the actualistic baseline for the analysis of long-term exhumation (Carrapa et al., 2003; Bernet and Garver, 2005), but the geologic interpretation of ancient sedimentary successions can be much more challenging due to a number of assumptions that can be difficult to test. In principle, the single-mineral contribution from each potential source area depends on the size of the eroding source, the propensity of the parent bedrock to yield the target mineral when exposed to erosion (mineral fertility – Moecher and Samson, 2006), and the rate of erosion on short-term time scale (Malusà et al., 2016a).

The European Alps, in the light of their well-known geologic evolution, are an excellent site to evaluate the combined impact of erosion rates and mineral fertility on the sedimentary record, and tackle this crucial issue for paleotectonic and paleoclimatic research (Fig. 1). Our study combines provenance discrimination based on the first trace-element and Nd-isotope analyses ever performed on the same detrital apatite grains, a state-of-the-art dataset of *in situ*-^{10}Be derived erosion rates (Wittmann et al., 2016), fission-track data and direct mineral fertility measurement (Malusà et al., 2016a). We chose to focus on apatite grains in modern sands of the Po river drainage because: (i) the Po River drains diverse tectonic domains shedding apatite grains with distinguishable chemical and isotopic fingerprints; (ii) the relatively small size of the Po basin allows us to fully determine all factors controlling the relative abundance of apatite grains with a reasonable effort; (iii) erosion in different orogenic segments is controlled by a different combination of endogenic and exogenic processes (Malusà and Vezzoli, 2006; Champagnac et al., 2009; Willett, 2010); and (iv) the Alps have been the subject of a number of lag-time studies that have led to contrasting interpretations, either in terms of steady state or episodic exhumation (e.g., Bernet et al., 2001; Carrapa et al., 2003; Carrapa, 2010).

Based on the recently published apatite fertility map of the European Alps (Malusà et al., 2016a), and on a comprehensive dataset of cosmogenic ^{10}Be concentration in quartz carried by all major tributaries of

the Po River (Wittmann et al., 2016), we calculate the expected percentage of apatite grains supplied to the Po delta from all the major Alpine and Apenninic eroding sources, and test these predictions by comparing them with the new high-resolution dataset of trace-element and Nd-isotope signatures on apatite grains. Fission-track analysis on selected samples is employed to test the robustness of the trace-element approach for provenance discrimination. Our results provide new insights on the main factors determining the single-mineral record of mountain erosion. Potentials and limitations of provenance studies based on single-mineral analyses, and the general implications for detrital thermochronology studies based on the lag-time approach are finally discussed.

2. Geologic setting

The Po river catchment drains a complex arcuate orogenic system formed on top of the subducting European plate, and including the accretionary wedge of the European Alps and its transition zone with the Northern Apennines (Fig. 1) (Handy et al., 2010; Malusà et al., 2015; Zhao et al., 2016). The Southalpine and Austroalpine units, exposed on the northern side of the drainage, represent the remnant of the Adriatic paleomargin of the Alpine Tethys, and were largely structured during Cretaceous Adria-Europe convergence (Zanchetta et al., 2015). This Cretaceous wedge forms a tectonic lid on top of the Cenozoic metamorphic units derived from the European paleomargin, i.e., the Lepontine dome of the Central Alps and the Paleogene accretionary wedge of the Western Alps, also including (U)HP units of Eocene age (Fig. 1). On the southern side of the Po river catchment, the Paleogene wedge includes the Ligurian units of the Northern Apennines, and is partly buried by wedge-top sedimentary successions (Malusà and Balestrieri, 2012). The underlying Subligurian and Tuscan units were accreted during Apenninic (Adriatic) subduction, and include Oligo-Miocene turbidites fed from the exhuming Lepontine dome and originally deposited in the Adriatic foredeep (Garzanti and Malusà, 2008; Anfinson et al., 2016). European continental crust that has escaped subduction during the Alpine orogeny is now exposed in the External Massifs of the Western and Central Alps.

Previous detrital thermochronology studies in the Po river catchment show that nearly half of the apatite grains found in modern sands of the Po delta display a young fission-track age (<10 Ma), which suggests provenance from bedrock units that have been eroded at high rates during the Neogene, such as the Lepontine dome, the External Massifs, and/or the Northern Apennines (Malusà et al., 2009a). Because of the variable climatic and tectonic conditions observed along different segments of the Alps-Apennines system, erosion in such areas is controlled by a different combination of endogenic and exogenic processes. In the high-relief Western Alps, slivers of European crust (e.g., the Mont Blanc External Massif) are tectonically extruded along major transpressional faults (Malusà et al., 2009b), and rapid erosion was possibly favoured by glacial processes (Valla et al., 2011). In

the medium-relief Central Alps, the Lepontine dome was indented and deeply unroofed since the late Oligocene (Malusà et al., 2016b). Previous work suggested that rock uplift in the Central Alps may reflect a positive feedback between denudation and isostatic response to erosional unloading (Champagnac et al., 2009), with erosion likely favoured by heavy precipitations (Frei and Schär, 1998). In the low-relief Northern Apennines, where precipitations and glacial impact are much less intense than in the Central Alps (Frei and Schär, 1998; Giraudi, 2004), erosion is most likely favoured by the high erodibility of the sedimentary successions exposed (e.g., Di Giulio et al., 2003).

3. Expected apatite contributions to the Po river system

In a modern drainage system, the expected contributions of different source areas to the total apatite load can be predicted if erosion rate and apatite fertility of each bedrock source are independently known. The apatite contribution is in fact proportional to the size of the source area, to the fertility of exposed bedrock, and to the short-term erosion rate. The apatite fertility map of the Po river system is shown in Figure 2a. Apatite fertility values, derived from the measurement of apatite concentration in modern sand samples (Malusà et al., 2016a), vary in the orogen from ~10 mg/kg to >2500 mg/kg. Values up to 2580 mg/kg characterize the Lepontine dome gneisses, whereas values are <100 mg/kg in the Northern Apennines, and lowest (11 to 29 mg/kg) in the sedimentary succession of the Southern Alps (Fig. 2a). High apatite fertility is observed in the continental crust of the External Massifs (667 to 944 mg/kg), the metamorphic units of the Cretaceous Austroalpine-Southalpine wedge (412 mg/kg), and part of the Paleogene wedge of the Western Alps (445 to 692 mg/kg in the Gran Paradiso unit), where apatite fertility generally ranges between 100 and 300 mg/kg. Variations in apatite fertility are thus much greater than variations in erosion rate expected in most orogenic belts, even in tectonic units with similar lithology and only showing different tectono-metamorphic evolution.

The erosion rate map of the Po drainage, derived from *in situ* ^{10}Be concentrations in quartz grains from modern sand samples (Wittmann et al., 2016), is shown in Figure 2b. These rates are quite variable along the orogen strike, but much less variable than apatite fertility. Values ≥0.6 mm/a are found in the northern Western Alps and in the Central Alps, with a maximum in the western Lepontine dome (~1.5 mm/a). Values <0.3 mm/a are found in most of the Southern Alps and in the southern Western Alps. Intermediate erosion rates (0.4-0.5 mm/a) characterize the Northern Apennines (Fig. 2b).

These data allows us to quantify the expected apatite contribution to the Po delta from different potential source areas (Fig. 2c and supplementary Table S1). The largest apatite contribution (~71%) is expected from the Lepontine dome, which combines high fertility, high erosion rates, and a large area. Significant apatite contributions are also expected from the Paleogene wedge of the Western

144 Alps (~12%) and from the metamorphic units of the Cretaceous wedge (~11%). Apatite contribution
145 from the External Massifs (~5% in total) is limited by the smaller exposure area, whereas apatite
146 contribution from the Northern Apennines and the sedimentary successions of the Southern Alps is
147 limited by the low fertility and moderate-to-low erosion rates despite the relatively large area.
148 Noteworthy, because of the high apatite fertility of the Lepontine rocks, the sediment contribution
149 from the Lepontine area (i.e, the apatite contribution divided by the relative apatite fertility) is
150 expected to be lower than the corresponding apatite contribution (~40% vs ~71%). By contrast,
151 sediment contributions from the Paleogene wedge (~28%) and the Northern Apennines (~18%) are
152 expected to be higher than the corresponding apatite contributions, because eroded rocks have low
153 apatite fertility (see supplementary Table S1).

154 **4. Rationale and methods**

155 We set up an experiment, based on trace-elements and Nd-isotope analyses on detrital apatite
156 grains from 14 modern river sands (samples S1-S11 and D1-D3 in Fig. 1), to independently test the
157 predictions of Fig. 2c. Trace element signatures of apatite grains have been applied for provenance
158 discrimination (Dill, 1994; Belousova et al., 2002; Morton and Yaxley, 2007), as well as Nd isotopes
159 (Allen et al., 2007; Foster and Carter, 2007; Henderson et al., 2010). Here, we apply both methods to
160 the same detrital grains. This approach is initially applied in combination with detrital fission-track
161 analysis to 3 selected rivers of the northern Western Alps. Because the Western Alps include two
162 main tectonic blocks (Eastern and Western blocks) with sharply distinct apatite fission-track
163 signatures (Resentini and Malusà, 2012), we analyzed one modern sand sample exclusively derived
164 from the Western block (Dora Baltea1-S5), one sample exclusively derived from the Eastern block
165 (Orco-S7), and one sample including detritus from both the Western and the Eastern blocks (Dora
166 Baltea2-S6). Using these three samples (marked by a star in Fig. 1), we performed two independent
167 provenance budgets based on the fission-track and geochemical signature of detrital apatite, and
168 compared the results. This allowed us to independently test the robustness of the geochemical
169 approach for provenance discrimination.

170 We then extended this approach to the whole Po river drainage, and analyzed 8 additional river
171 sand samples to characterize each tectonic domain exposed within the catchment: Cretaceous wedge
172 (Adda-S1), Lepontine dome (Ticino-S2, Maggia-S3, Toce-S4), metamorphic Western Alps (Dora
173 Riparia-S8, Varaita-S9), External Massifs (Stura di Demonte-S10), and Ligurian units of the
174 Apennines (Scrivia-S11). We avoided samples derived from the Subligurian and Tuscan units of the
175 Northern Apennines, because these units largely derive from the erosion of the Lepontine dome
176 (Garzanti and Malusà, 2008; Anfinson et al., 2016), and include recycled apatite grains that are not
177 distinguishable on a geochemical ground from those shed from the Central Alps. We finally analyzed

three sand samples from three different sites of the Po delta (D1 to D3) (see Supplementary Table S2 for further details on sample locations). Unlike pioneering studies comparing detrital apatite Nd values with source whole-rock values (Foster and Carter, 2007), our approach, similarly to the one described in Henderson et al. (2010), allows to directly compare Nd data in detrital apatite among source and sink areas. Moreover, it additionally relies on independent constraints provided by trace element data on the same grains, by ^{10}Be-derived erosion rates, and by mineral fertility determinations.

Apatite grains were concentrated in the laboratory of Milano-Bicocca University according to the procedure described in Malusà et al. (2016a), after modelling the expected amount of apatite grains found in different grain-size classes on the basis of settling-equivalence relationships (Resentini et al., 2013). We performed a hydrodynamic pre-concentration of dense mineral grains using a Gemeni shaking table, and extracted the dense fraction by centrifuging in sodium polytungstate diluted at 2.90 kg/dm^3. The dense mineral concentrate was further refined with a Frantz magnetic separator under an increasing field strength up to 0.6 A, and the diamagnetic dense fraction was then passed in glassware through liquid diiodomethane (3.32 kg/dm^3). The apatite concentrate from each sample was split in two different aliquots. An aliquot was embedded in epoxy resin, polished, and prepared for fission-track analysis according to the external detector method (see supplementary material for details). Another aliquot was analyzed for trace elements and Nd isotopes. Apatite grains free of visible inclusions and major fractures were hand-picked and mounted in 2.5 cm diameter epoxy resin discs, and then polished to expose the internal surface of the grains.

Trace element and Nd isotope compositions were determined by LA–ICP–MS at the Institute of Geology and Geophysics, Chinese Academy of Sciences, Beijing. For trace elements, we followed a procedure similar to that described by Xie et al. (2008) for zircon. We utilized an Agilent 7500a Q–ICP–MS that adopts an abaxial Omega II lens system, and a laser ablation system consisting of a Coherent ArF excimer laser generator with wave length of 193 nm and a laser optical system with a laser beam homogenizing system (laser spot size: 5 to 160 μm; frequency: 1 to 20 Hz; energy density up to 45 J/cm^2). Prior to routine analysis, a tuning solution was used to optimize the ICP–MS, and the pulse/analog factor of the detector was corrected to adjust the linearity between the pulse and the analogue signal mode. During laser ablation, helium was used as the carrier gas and mixed with argon prior to entering the ICP torch. The parameters of the two gases were optimized by using continuous ablation of NIST SRM 610 glass in order to get stable maximum signal intensity while suppressing oxide formation, which was monitored using signals of $^{238}U^+$ and $^{238}U^{16}O^+/^{238}U^+$ ($^{238}U^+ > 4{,}000$ cps/ppm, $^{238}U^{16}O^+/^{238}U^+ < 0.5\%$). Ablation operated at 15 J/cm^2 with laser pulse frequency of 8 Hz, using a spot size of 60 μm. Each spot analysis consists of approximately 15 s background acquisition

and 50 s sample data acquisition. The ICP–MS measurement was carried out by using time-resolved analysis and peak hopping at one point per mass. The dwell time was 0.006 s for each trace element. Trace element concentrations were calibrated against NIST SRM 610 as the external reference material, using Ca as an internal standard element with GLITTER 4.0. The concentration of Ca for each sample was determined by electron microprobe.

Apatite grains with Nd >350 ppm were fully characterized also in terms of Nd isotopes. *In situ* Nd isotope compositions were determined by using a Neptune MC–ICP–MS coupled with the 193 nm ArF excimer laser system. This double-focusing multicollector ICP–MS has the capability of high mass resolution measurements in multiple collector mode. It is equipped with eight motorized Faraday cups and one fixed central channel, where the ion beam can be switched between Faraday and SEM detector. All Faraday cups are sequentially connected to all amplifiers, to remove gain calibration errors and improve the external precision of the measurements (Wu et al., 2006). We followed the analytical protocol, experimental conditions and cup configurations given by Yang et al. (2008). A JNdi-1 standard solution was used to calibrate the instrument before routine analysis. The average JNdi-1 $^{143}Nd/^{144}Nd$ ratio obtained (0.512099 ± 0.000012; 2σ, n = 6), is identical within error to the recommended range of 0.512115 ± 0.000007 by ID–TIMS (Tanaka et al., 2000). For laser ablation analyses, the spot size was 90–120 μm with an 8 Hz laser pulse frequency. To precisely determine the isobaric interference of ^{144}Sm on ^{144}Nd, the β_{Sm} value was directly obtained from the $^{147}Sm/^{149}Sm$ ratio on the sample itself, following the method proposed by McFarlane and McCulloch (2007). For isobaric correction, we used the values of 1.08680 for $^{147}Sm/^{149}Sm$ (Dubois et al., 1992) and 0.22332 for $^{144}Sm/^{149}Sm$ (Isnard et al., 2005). The $^{143}Nd/^{144}Nd$ and $^{145}Nd/^{144}Nd$ ratios were corrected for mass bias using the exponential law (Russell et al., 1978), assuming $^{146}Nd/^{144}Nd$ = 0.7219 for calculation of the mass bias factor. The stable $^{145}Nd/^{144}Nd$ ratio was used to evaluate the feasibility of our analyses, because it has a constant value of 0.348415 obtained by TIMS (Wasserburg et al., 1981). The in-house apatite standard (AP2) yielded average $^{143}Nd/^{144}Nd$ ratios of 0.510986±49 (2σ, n = 37), in line with the value of 0.510985 ± 8 (2σ) obtained by the purified solution method of MC–ICP–MS analysis. The obtained average $^{145}Nd/^{144}Nd$ ratios of 0.348405 ± 36 (2σ, n = 37) are also identical to the recommended value of 0.348415 (Wasserburg et al., 1981).

Apatite grains yielding anomalously high Zr concentrations, which may indicate ablation of undetected zircon inclusions, and non-apatite grains recognized by their anomalous REE patterns, were both discarded from the dataset. The final dataset that we used to produce discrimination plots includes 871 apatite grains fully characterized in terms of trace element composition, and 296 apatite grains additionally characterized for their Nd isotope composition.

5. Results

246 ***5.1 Trace-element data***

247 The trace-element dataset is synthesized in Figures 3 to 5a, and is reported in full in supplementary
248 Table S3. Figure 3 shows the median values of the chondrite-normalised trace element patterns in
249 each sample (see supplementary Fig. S1 for single-grain spider diagrams).

250 The trace-element data of the three replicate Po delta samples (thick gray lines in Fig. 3) show
251 consistent patterns with MREE enrichment and a strong Eu anomaly. Similar trends are shown by the
252 Adda (S1), Ticino (S2) and Orco (S7) samples, derived from the Cretaceous wedge, Lepontine dome
253 and (U)HP belt of the Paleogene wedge, respectively. Apatite grains from the External Massifs (Dora
254 Baltea1-S5 and Stura di Demonte-S10) display higher LREE and stronger Eu anomaly than apatite
255 grains from the Po delta. A substantial difference in HREE can be observed between the more
256 depleted apatites derived from the Mont Blanc Massif (MB, sample S5 in Fig. 1) and those derived
257 from the Argentera Massif (AG, sample S10 in Fig. 1). Unlike the Ticino River, other rivers draining
258 the Lepontine dome (Maggia-S3 and Toce-S4) carry apatite grains more depleted in LREE and with
259 a weaker Eu anomaly compared to samples D1-D3. Weak Eu anomalies are also found, on average,
260 in apatites derived from other segments of the Paleogene wedge (Dora Riparia-S8, Varaita-S9,
261 Scrivia-S11). Sample S8 is also characterized by strongly REE-enriched apatite grains.

262 In the light of the observed trace-element variations in apatite grains from different samples,
263 parameters relevant for provenance discrimination, such as Y vs ΣREE and (La/Yb)N vs (Gd/Yb)N,
264 were plotted in Figures 4 and 5 (see also supplementary Fig. S2 for a wider set of diagrams). Focusing
265 on the northern Western Alps, i.e., on the Dora Baltea and adjacent Orco catchments (samples S4 to
266 S6 in Fig. 1), we observe that apatite grains from the External Massifs (red dots in Fig. 4) and from
267 the metamorphic wedge (blue dots in Fig. 4) are geochemically distinct. The apatite grains from the
268 External Massifs define steeper trends, both in the Y vs ΣREE diagram and in the (La/Yb)N vs
269 (Gd/Yb)N diagram. In sample S6 (large gray dots in Fig. 4), trace-element data show that apatite
270 grains from the External Massifs and the metamorphic wedge are combined in a proportion
271 approximately 2:3.

272 The same proportion is obtained by fission-track data (see supplementary Fig. S3), which allows
273 us to perform an independent provenance budget on the same samples, because apatite grains have a
274 much younger cooling age in the External Massifs (red distributions in Fig. 4) than in the
275 metamorphic wedge (blue distributions in Fig. 4). Apatite grains from these two different tectonic
276 domains are combined in sample S6, which yielded a bimodal grain-age distribution with two
277 populations encompassing 43% and 57% of dated grains, respectively.

278 The consistency between the results obtained in the northern Western Alps by using trace-element
279 and fission-track data allows us to safely extrapolate the trace-element provenance approach to the

entire Po drainage. At the scale of the entire basin, we observe an equally marked difference between apatite grains shed from the External Massifs (red dots in Fig. 5a) and those shed from the Lepontine dome (green dots in Fig. 5a). However, apatite grains shed from the Lepontine dome partly overlap grains derived from the Cretaceous and Paleogene wedges (brown and blue dots in Fig. 5a, respectively). The trace-element distribution on apatite from tributary samples consistently matches the distribution observed in the Po delta, apart from sample S8 (Dora Riparia), which shows a higher Y concentration. In the (La/Yb)N vs (Gd/Yb)N diagram, the different slope defined by apatites derived from the External Massifs and the Lepontine dome is consistent with the relative HREE depletion in the former relative to the latter. Although most of the apatite grains from the Po delta apparently fit a Lepontine or an External Massif source, the (La/Yb)N vs (Gd/Yb)N diagram also shows that part of the Po delta apatite grains (i.e., those on the top right part of the diagram, Fig. 5a) are exclusively consistent with a Paleogene wedge source.

Trace-element diagrams of supplementary Fig. S2 show that the apatite grains derived from the External Massifs have relatively high concentrations in Ce and U, and lower Eu/Eu* values compared to apatite grains derived from the Lepontine source area. Supplementary Figure S2 also shows that the lowest U concentrations are found in apatite grains from the Paleogene wedge. Among the Paleogene wedge sources, the apatite grains derived from the Dora Riparia catchment are easily distinguished for their higher concentration in Mn and total REE, and for their high Th/U ratio.

The Y vs ΣREE diagram of Fig. 5a, and the corresponding discrimination diagram of supplementary Figure S3, show that the distribution of most Po delta apatite grains matches the combined distributions of apatite from the Lepontine dome (in green) and the Mont Blanc – Argentera External Massifs (in red). The same systematic overlap is observed in other discrimination diagrams of Figure S3 (e.g., Th vs Ce; (La/Yb)N vs ΣREE; Y vs Eu/Eu*; (La/Yb)N vs Y). In the same diagrams, the fields of observed trace-element concentrations and ratios for the Paleogene wedge are clearly independent from the trends shown by apatite grains in the Po delta (see, e.g., the (La/Yb)N vs ΣREE and the Y vs Eu/Eu* diagrams in supplementary Fig. S3). The role of the Cretaceous wedge is more difficult to assess, because fields of the Cretaceous wedge largely overlap those of the Lepontine dome, and are systematically nested within the fields of the Paleogene wedge.

The distribution of data points in 11 different discrimination diagrams based on different combinations of trace-element parameters (supplementary Fig. S3) suggests that the Po delta apatite record is dominated by Lepontine sources, with potential minor contributions from the External Massifs. Moreover, the (La/Yb)N vs (Gd/Yb)N, U vs (La/Yb)N, and U vs Th/U discrimination diagrams (see Fig. S3) show that part of the apatite grains in the delta is ascribed to the Paleogene wedge (>10% according to the (La/Yb)N vs (Gd/Yb)N diagram). When these discrimination

diagrams are considered individually, the percentage of Po delta apatites consistent with a Lepontine dome provenance is calculated not to exceed 73% (pale green squares in Fig. 6a). The maximum value expected for the Mont Blanc and Argentera External Massifs does not exceed 24% (pale red squares in Fig. 6a). Because of the partly overlapping Lepontine and External Massifs discrimination fields, the maximum total amount of apatite grains ascribed to these sources is constrained to ≤85% (gray squares in Fig. 6a). Results are significantly improved when the same discrimination diagrams are applied sequentially (dark squares in Fig. 6a), that is, when each grain simultaneously fits all of the 11 discrimination fields derived from the different combinations of trace-element parameters listed in Fig. 6a. In this latter case, the apatite contribution is calculated not to exceed 62% and 13% for the Lepontine dome and the External Massifs, respectively (dark green and dark red squares in Fig. 6a). The maximum total amount of apatite grains ascribed to these sources is constrained to ≤69% (black square in Fig. 6a), but the real values may be lower because of the potential contributions from the Cretaceous and Paleogene wedges.

5.2 Nd-isotope data

The Nd-isotope dataset is synthesized in Figure 5b, and reported in full in supplementary Table S4. Apart from sample S8, ~20 to 60% of the total analyzed grains in each sample yielded Nd concentrations >350 ppm, which is sufficiently high to characterize the same grains in terms of Nd isotopic composition. Figure 5b shows the *in situ* Sm-Nd isotopic data both in terms of Nd ratios, and as model age vs ε_{Nd} (ε_{Nd} is parts per 10,000 variation of the $^{143}Nd/^{144}Nd$ ratio from the chondritic uniform reservoir). We calculated two-stage Nd-isotopic model ages for the eroded rock units, largely consisting of continental crust, under the assumption that a significant change in Sm/Nd ratio has occurred during the Variscan orogeny, i.e., after extraction from the mantle.

The Nd isotopic compositions in apatite grains from tributary samples consistently match the distribution observed in grains from the Po delta (in gray in Fig. 5b). In the $^{143}Nd/^{144}Nd$ vs $^{147}Sm/^{144}Nd$ diagram, apatites from the External Massifs show a gently dipping trend. Most of the $^{143}Nd/^{144}Nd$ ratios range from 0.5118 to 0.5126, with values even >0.5130 in apatite derived from the Paleogene wedge, whereas the $^{147}Sm/^{144}Nd$ ratios are generally higher in apatite grains derived from Lepontine sources than in apatite grains derived from the External Massifs. These latter grains generally exhibit Nd-isotopic model ages in the range of 1 to 2 Ga, but model ages may reach values approaching 3 Ga in samples from the Lepontine area, and are occasionally <1 Ga in samples from the Paleogene wedge.

According to the Nd-isotopic signatures of Fig. 5b, and the associated discrimination diagrams of supplementary Figure S4, apatite grains derived from Lepontine sources may range from a minimum of 46% to a maximum of 76% in sand of the Po delta (green bar in Fig. 6b), whereas the External

Massifs may supply a maximum of 33% apatite grains (red bar in Fig. 6b). However, a bias in these estimates is introduced by the different percentage of Nd-rich apatite grains shed from the different source areas (gray lozenges in Fig. 6b). In the Po delta, only grains with Nd >350 ppm can be fully characterized in terms of Nd isotopes. Because these Nd-rich grains are much less in the Lepontine dome (22%) than in the External Massifs (86%), Nd-isotope data will underestimate the apatite contribution from the Lepontine dome compared to the External Massifs.

The Nd-isotope discrimination fields of the External Massifs show a substantial overlap with those of the Cretaceous wedge (see supplementary Fig. S4), potentially accounting for 4 to 41% of total apatite grains found in the Po delta (brown bar in Fig. 6b). Apatite from the Paleogene wedge, according to Nd-isotope data, must represent at least 9%, and 32% at most of total apatite grains (blue bar in Fig. 6b). Noteworthy, these loosely constrained detrital sources are not able to contribute apatite grains with young fission-track ages to the Po delta (Malusà et al., 2009a).

5.3 Provenance budget and comparison with predictions based on cosmogenic nuclide and fertility data

A provenance budget based on combined trace-element and Nd-isotope data in sand of the Po delta is shown in Fig. 7. The estimated apatite contribution from the Lepontine sources ranges between 46% and 62%. The lower boundary of this range, which is based on Nd-isotope data, is possibly underestimated due to the low percentage of Nd-rich apatite grains characterizing the Lepontine source rocks. Apatite with the same fingerprint may derive also from the Subligurian and Tuscan units of the Northern Apennines (Malusà et al., 2016b), but the potential contribution from these latter sources is limited by their low fertility. The sum of all of the other sources contributing apatite to the Po delta cannot exceed 54% of all apatite grains. Those from the Paleogene wedge may range from 10% to 32%, with negligible contribution from the Dora Riparia catchment. This contribution is possibly overestimated, because of the high percentage of Nd-rich apatite grains observed in the Paleogene wedge. The contribution from the Mont Blanc and Argentera External Massifs may range between 0% and 13%, but cannot exceed two thirds of the apatite contribution from the whole Paleogene wedge. Apatite contribution between 4% and 41% from the Cretaceous wedge is loosely constrained, because of the substantial overlap with the discrimination fields of other potential sources.

These results are consistent with the trace-element patterns shown in spider diagrams of Fig. 3. The Po delta samples D1 to D3 consistently show MREE enrichment and strong Eu anomaly. Similar trends are also shown by tributaries draining the Lepontine dome (Ticino-S2), the Cretaceous wedge (Adda-S1) and the Paleogene wedge of the northern Western Alps (Orco-S7), thus confirming the results provided by discrimination plots. Apatite grains derived from the External Massifs (S5 and

S10) display higher LREE and stronger Eu anomaly than the median values observed in the Po delta, in line with a lower apatite contribution from these sources.

Predicted apatite contributions derived from cosmonuclide and mineral-fertility data are also indicated in Figure 7. They systematically match with the range independently derived from trace-element and Nd-isotope data, and point to dominant apatite contribution from the Lepontine dome (70.8%), well subordinate contributions from the Paleogene and Cretaceous wedges (11.8% and 10.8%, respectively), and minor contributions from the External Massifs (5%). Therefore, predictions based on apatite geochemistry, i.e., from a very small fraction of the bulk sediment (from 0.0002% to 0.25%), are fully consistent with predictions based on *in situ* ^{10}Be concentrations measured on quartz grains, which represent ~30 to >50 weight % of the analyzed samples.

6. Discussion

6.1 General implications for single-mineral detrital studies

The detrital archive provides an accurate record of mountain erosion that preserves key information for paleotectonic and paleoclimatic reconstructions (Najman, 2006; Garzanti et al., 2011). Single-mineral analyses of accessory phases (e.g., apatite and zircon) are increasingly employed in detrital studies because they minimize the effects of hydraulic sorting and differential diagenetic dissolution (von Eynatten and Dunkl, 2012). However, their interpretation is far from straightforward, because the impact of each eroding source on the detrital record is controlled by a range of factors also including the mineral fertility of eroded bedrock (Moecher and Samson, 2006; Vezzoli et al., 2016). In this study, we performed indipendent provenance budgets based both on apatite geochemical/isotopic fingerprints, and *in situ* ^{10}Be concentration in quartz grains from the same samples (Wittmann et al., 2016). The analysis of our datasets demonstrates that single-mineral methods on accessory minerals, when correctly applied and complemented with mineral fertility measurements (Malusà et al., 2016a), provide results that are fully consistent with those provided by the analysis of much more abundant framework minerals (e.g., quartz) (see Fig. 7).

This study also highlights a remarkable consistency in provenance discriminations based on independent analytical techniques on the same accessory phase, i.e., fission-track and geochemical analyses on detrital apatite grains. This confirms and extends the suggestion by previous works (Foster and Carter, 2007; Henderson et al., 2010) that the trace-element and Nd-isotope signatures of detrital apatite represent a reliable tool to disentangle the complex single-mineral record of orogenic erosion. Budgets based on Nd-isotopic fingerprints may be biased by the different percentage of Nd-rich apatite grains shed from different source areas. However, this potential source of bias can be evaluated and fully accounted for by a combined application of Nd-isotope and trace-element analyses on the same grains.

6.2 Implications for the lag-time approach to detrital thermochronology

The lag-time approach utilizes the difference between the cooling age and the depositional age of detrital minerals, and its trend throughout a stratigraphic succession, to provide information about the long-term exhumation history of an orogenic belt (Garver et al., 1999; Ruiz et al., 2004). In lag-time studies, attention is generally focused on the youngest grain-age population of the mineral under consideration (e.g., zircon, apatite or mica) (Carrapa et al., 2003; Bernet et al., 2009). In modern sands, the depositional age is equal to zero, and the lag time is thus equal to the age of the grain-age population under consideration.

Previous detrital thermochronology analyses in the Po river catchment show that nearly half of the apatite grains found in modern sands of the Po delta belong to a young (7.7 Ma) grain-age population (Malusà et al., 2009a) potentially including apatite shed from the External Massifs, the Lepontine dome and/or the Northern Apennines (Fig. 8). Because a different combination of exogenic and endogenic processes is believed to control the erosional exhumation of these different source areas (Champagnac et al., 2009; Malusà and Balestrieri, 2012; Malusà et al., 2016a), provenance of apatite grains forming this young age peak should be independently assessed. This may allow to understand which orogenic segment and which set of processes is reflected in the detrital record, and possibly monitored by a thermochronology study based on the lag-time approach. Provenance discriminations, either based on double- or triple-dating (Zattin et al., 2012; Danišík et al., 2017), or on trace-element and isotopic analyses of the same detrital grains dated by thermochronologic methods (Carter, 2007; Henderson et al., 2010), may thus represent a valuable support to detrital thermochronology studies, and should be generally applied to assess which orogenic source and set of processes is reflected in the single-mineral record preserved in the final sediment sink. Trace-element and isotopic fingerprints may survive burial diagenesis, and may be applied for provenance discrimination not only to modern sands, but also to older sedimentary successions.

Our trace-element and Nd-isotope data show that the large majority of apatite grains in the Po delta derives from the Lepontine dome, with negligible contributions from the External Massifs and the Northern Apennines (Fig. 7). This implies an almost exclusive Lepontine origin for the youngest fission-track age population found in the Po delta (Fig. 8). This finding implies that the apatite single-mineral approach to the analysis of the Po delta samples does not provide valuable information on relevant tectonic processes taking place in other orogenic segments lying within the Po drainage. For example, the fast tectonically-driven exhumation of the Mont Blanc Massif, the highest mountain in Europe, can be readily traced in detritus of the Dora Baltea catchment (Fig. 4), but is diluted and almost completely blurred in the detrital record at the scale of the whole Po basin. This is also the case of the fast Pliocene-Quaternary exhumation of the Northern Apennines.

In general terms, although lag-time analysis is often used to infer the long-term evolution of an entire mountain range, it is important to note that it emphasizes the cooling history of areas characterized by high mineral fertility. Because mineral fertility across a mountain belt can vary regionally over several orders of magnitude (see, e.g., Fig. 2a), parts of an orogenic belt may be not represented in the detrital thermochronology record. Whenever the assumption of uniform mineral fertility is not reasonable, the geologic interpretation of detrital thermochronology data would thus benefit from a careful mineral fertility characterization of the potential source areas.

An example of lag-time analysis potentially biased by uneven mineral fertility in the source areas is provided by the European Alps, where major changes in fertility are documented not only for apatite, but also for zircon (Malusà et al., 2016a). Fertility values derived from the measurement of zircon concentration in modern sand samples vary from ~0.4 mg/kg to ~90 mg/kg. Values up to ~70-90 mg/kg characterize the Lepontine dome and the External Massifs, whereas much lower values invariably <10 mg/kg, and in places as low as 0.4 mg/kg, characterize the Paleogene wedge of the Western Alps, the Southern Alps and the Northern Apennines (Malusà et al., 2016a, their Fig. 11). The detrital-zircon thermochronology record in detritus derived from the Alps is thus largely determined by zircon grains derived from the high-fertility rocks of the Lepontine dome and the External Massifs.

Previous studies based on the lag-time analysis of Alpine-derived detrital zircon in Oligocene-Miocene sedimentary rocks (Bernet et al., 2001, 2009) have inferred a steady-state exhumation of the whole European Alps over the last 30 Myr. However, the Lepontine dome was the only high-fertility source area that contributed zircon grains potentially recording Oligocene–Miocene exhumation to the analyzed sedimentary rocks. The External Massifs were still buried beneath thick sedimentary strata during the Oligocene and part of the Miocene (Garzanti and Malusà, 2008), and zircon grains eroded from these strata may record older exhumation events of distant sediment sources (e.g., Rahl et al., 2007) rather than the exhumation of the External Massifs. This implies that the lag-time analysis of Alpine-derived detrital zircon preserved in the final sediment sink might provide evidence, at best, for a steady state exhumation of the Lepontine dome, not of the entire European Alps. This does not exclude the possibility of orogen-wide steady state over the last 30 Myr (Bernet et al., 2001), but it means that this possibility cannot be demonstrated by using a dataset that provides information on a small part of the orogenic belt only (i.e., the Lepontine dome). The exhumation of the Lepontine dome, one of the best-studied areas of the Alps, has long been recognized to proceed stepwise from east to west within different subdomes (Schlunegger and Willett, 1999; Garzanti and Malusà, 2008; Anfinson et al., 2016; Malusà et al. 2016b). Therefore, it cannot be considered to have proceeded in

steady state through time, unlike suggested by available lag-time trends in Oligocene-Miocene sedimentary rocks of the final sink.

7. Conclusions

Our analysis of the single-mineral record of Alpine erosion, which combines apatite provenance discrimination based on trace-element and Nd-isotope analyses independently validated by fission-track dating, with direct measurement of apatite fertility and *in situ*-^{10}Be derived erosion rates, led to the following main conclusions:

1) trace-element and Nd-isotope fingerprints of detrital apatite grains represent a powerful tool to disentangle the complex record of orogenic erosion, as independently confirmed by fission-track data. Application to the Po river catchment shows that the majority of apatite grains in the Po delta derives from the Lepontine dome in the Central Alps;
2) the single-mineral record in the final sediment sink can be largely determined by high-fertility source rocks exposed within the drainage; the detrital thermochronology record may thus reflect processes affecting relatively small parts of the orogenic system under consideration, and may underrepresent major orogenic segments even characterized by fast erosion that only have a low mineral fertility;
3) detrital thermochronology studies based on the lag-time approach may benefit from a mineral fertility characterization of the potential source areas, and should include independent provenance discriminations of dated mineral grains; this would allow a correct identification of the sediment sources, leading to an improved geologic interpretation of the detrital thermochronology record preserved in the final sediment sink.

In the light of our results, many previous interpretations of detrital thermochronology datasets in terms of orogenic-wide steady state might be proficiently reconsidered.

Acknowledgments.

This work benefitted from insightful comments by M. Zattin and an anonymous reviewer, from discussions with M.L. Balestrieri, P.G. Fitzgerald and A. Resentini, and from comments on an early version of the manuscript by M.T. Brandon and an anonymous reviewer. D. Alami, M. Fornara, M. Limoncelli, C. Pellicioli, P. Piazza, G. Tango and F. Tangocci contributed to mineral separation. Cosmogenic nuclide analyses funded by DFG Project WI 3874/3-1 to H.W. and M.G.M.

References

1. Allen, R., Carter, A., Najman, Y., Bandopadhyay, P.C., Chapman, H. J., et al., 2007. New constraints on the sedimentation and uplift history of the Andaman-Nicobar accretionary prism, South Andaman Island. Geol. Soc. Am. Special Paper 436, 223-256.

2. Anfinson, O. A., Malusà, M. G., Ottria, G., Dafov, L. N., Stockli, D. F., 2016. Tracking coarse-grained gravity flows by LASS-ICP-MS depth-profiling of detrital zircon (Aveto Formation, Adriatic foredeep, Italy). Mar. Petrol. Geol. 77, 1163-1176.

3. Belousova, E.A., Griffin, W,L,, O'Reilly, S.Y., Fisher, N.I., 2002. Apatite as an indicator mineral for mineral exploration: trace-element compositions and their relationship to host rock type. J. Geochem. Explor. 76, 45-69.

4. Bermúdez, M. A., van der Beek, P. A., Bernet, M., 2013. Strong tectonic and weak climatic control on exhumation rates in the Venezuelan Andes. Lithosphere 5(1), 3-16.

5. Bernet, M., Garver, J. I., 2005. Fission-track analysis of detrital zircon. Rev. Mineral. Geochem. 58(1), 205-237.

6. Bernet, M., Zattin, M., Garver, J. I., Brandon, M. T., Vance, J. A., 2001. Steady-state exhumation of the European Alps. Geology 29(1), 35-38.

7. Bernet, M., Brandon, M., Garver, J., Balestieri, M. L., Ventura, B., Zattin, M., 2009. Exhuming the Alps through time: Clues from detrital zircon fission-track thermochronology. Basin Res. 21(6), 781-798.

8. Carrapa, B., Wijbrans, J., Bertotti, G., 2003. Episodic exhumation in the Western Alps. Geology 31(7), 601-604.

9. Carrapa, B., 2010. Tracing exhumation and orogenic wedge dynamics in the European Alps with detrital thermochronology: REPLY. Geology 38(11), e227.

10. Carter, A., 2007. Heavy minerals and detrital fission-track thermochronology. Dev. Sediment. 58, 851-868.

11. Champagnac, J. D., Schlunegger, F., Norton, K., von Blanckenburg, F., Abbühl, L. M., Schwab, M., 2009. Erosion-driven uplift of the modern Central Alps. Tectonophysics 474(1), 236-249.

12. Danišík, M., McInnes, B.I., Kirkland, C.L., McDonald, B.J., Evans, N.J., Becker, T., 2017. Seeing is believing: Visualization of He distribution in zircon and implications for thermal history reconstruction on single crystals. Science Advances 3, e1601121.

13. Di Giulio, A., Ceriani, A., Ghia, E., Zucca, F., 2003. Composition of modern stream sands derived from sedimentary source rocks in a temperate climate (Northern Apennines, Italy). Sed. Geol.158, 145-161.

14. Dill, H.G., 1994. Can REE patterns and U-Th variations be used as a tool to determine the origin of apatite in clastic rocks. Sediment. Geol. 92, 175-196.

15. Dubois, J.C., Retali, G., Cesario, J., 1992. Isotopic analysis of rare earth elements by total vaporization of samples in thermal ionization mass spectrometry. Int. J. Mass Spectr. Ion Proc. 120, 163–177.

16. Foster, G.L., Carter, A., 2007. Insights into the patterns and locations of erosion in the Himalaya - A combined fission-track and in situ Sm–Nd isotopic study of detrital apatite. Earth. Planet. Sci. Lett. 257, 407-418.

17. Frei, C., Schär, C., 1998. A precipitation climatology of the Alps from high-resolution rain-gauge observations. Int. J. Climat. 18(8), 873-900.

18. Garver, J. I., Brandon, M. T., Roden-Tice, M., Kamp, P. J., 1999. Exhumation history of orogenic highlands determined by detrital fission-track thermochronology. Geol. Soc. London Spec. Publ. 154(1), 283-304.

19. Garzanti, E., Malusà, M. G., 2008. The Oligocene Alps: Domal unroofing and drainage development during early orogenic growth. Earth Planet. Sci. Lett. 268(3), 487-500.

20. Garzanti, E., Vezzoli, G., Andò, S., 2011. Paleogeographic and paleodrainage changes during Pleistocene glaciations (Po Plain, northern Italy). Earth-sci. Rev., 105(1), 25-48.

21. Garzanti, E., Resentini, A., Vezzoli, G., Andò, S., Malusà, M.G., Padoan, M., 2012. Forward compositional modelling of Alpine orogenic sediments. Sediment. Geol. 280, 149-164.

22. Giraudi, C., 2004. The Apennine glaciations in Italy. Quarternary glaciations–extent and chronology, part I: Europe. Dev. Quaternary Sci. 2, 215-224.

23. Handy, M. R., Schmid, S. M., Bousquet, R., Kissling, E., Bernoulli, D., 2010. Reconciling plate-tectonic reconstructions of Alpine Tethys with the geological–geophysical record of spreading and subduction in the Alps. Earth-Sci. Rev. 102, 121–158.

24. Henderson, A.L., Foster, G.L., Najman, Y., 2010. Testing the application of in situ Sm–Nd isotopic analysis on detrital apatites: a provenance tool for constraining the timing of India–Eurasia collision. Earth. Planet. Sci. Lett. 297, 42–49.

25. Huntington, K. W., Blythe, A. E., Hodges, K. V., 2006. Climate change and Late Pliocene acceleration of erosion in the Himalaya. Earth Planet. Sci. Lett. 252(1), 107-118.

26. Isnard, H., Brennetot, R., Caussignac, C., Caussignac, N., Chartier, F., 2005. Investigations for determination of Gd and Sm isotopic compositions in spent nuclear fuels samples by MC ICPMS. Int. J. Mass Spectr. 246, 66–73.

27. Malusà, M. G., Vezzoli, G., 2006. Interplay between erosion and tectonics in the Western Alps. Terra Nova 18(2), 104-108.

28. Malusà, M. G., Balestrieri, M. L., 2012. Burial and exhumation across the Alps-Apennines junction zone constrained by fission-track analysis on modern river sands. Terra Nova 24, 221–226.

29. Malusà, M. G., Zattin, M., Andò, S., Garzanti, E., Vezzoli, G., 2009a. Focused erosion in the Alps constrained by fission-track ages on detrital apatites. Geol. Soc. London Spec. Publ. 324(1), 141-152.

30. Malusà, M. G., Polino, R., Zattin, M., 2009b. Strain partitioning in the axial NW Alps since the Oligocene. Tectonics 28, TC002370, 1-26.

31. Malusà, M. G., Faccenna, C., Baldwin, S. L., Fitzgerald, P. G., Rossetti, F., Balestrieri, M. L., Danišík, M., Ellero, A., Ottria, G., Piromallo, C., 2015. Contrasting styles of (U)HP rock exhumation along the Cenozoic Adria-Europe plate boundary (Western Alps, Calabria, Corsica). Geochem. Geophys. Geosyst. 16, 1786-1824.

32. Malusà, M. G., Resentini, A., Garzanti, E., 2016a. Hydraulic sorting and mineral fertility bias in detrital geochronology. Gondwana Res., 31, 1-19.

33. Malusà, M. G., Anfinson, O. A., Dafov, L. N., Stockli, D. F., 2016b. Tracking Adria indentation beneath the Alps by detrital zircon U-Pb geochronology: Implications for the Oligocene–Miocene dynamics of the Adriatic microplate. Geology 44(2), 155-158.

34. McFarlane, C.R.M., McCulloch, M.T., 2007. Coupling of in-situ Sm\Nd systematics and U–Pb dating of monazite and allanite with applications to crustal evolution studies. Chem. Geol. 245, 45–60.

35. Moecher, D. P., Samson, S. D., 2006. Differential zircon fertility of source terranes and natural bias in the detrital zircon record: Implications for sedimentary provenance analysis. Earth Planet. Sci. Lett. 247(3), 252-266.

36. Morton, A., Yaxley, G., 2007. Detrital apatite geochemistry and its application in provenance studies. Geol. Soc. Am. Special Paper 420, 319-344.

37. Najman, Y., 2006. The detrital record of orogenesis: A review of approaches and techniques used in the Himalayan sedimentary basins. Earth-Sci. Rev. 74(1), 1-72.

38. Rahl, J. M., Ehlers, T. A., van der Pluijm, B. A., 2007. Quantifying transient erosion of orogens with detrital thermochronology from syntectonic basin deposits. Earth Planet. Sci. Lett. 256(1), 147-161.

39. Resentini, A., Malusà, M. G., 2012. Sediment budgets by detrital apatite fission-track dating (Rivers Dora Baltea and Arc, Western Alps). Geol. Soc. Am. Special Papers 487, 125-140.

40. Resentini, A., Malusà, M. G., Garzanti, E., 2013. MinSORTING: An Excel® worksheet for modelling mineral grain-size distribution in sediments, with application to detrital geochronology and provenance studies. Computers Geosci. 59, 90-97.

41. Ruiz, G., Seward, D., Winkler, W., 2004. Detrital thermochronology–a new perspective on hinterland tectonics, an example from the Andean Amazon Basin, Ecuador. Basin Res. 16, 413-430.

42. Russell, W.A., Papanastassiou, D.A., Tombrello, T.A., 1978. Ca isotope fractionation on the Earth and other solar system materials. Geochim. Cosmochim. Acta 42, 1075–1090.

43. Schlunegger, F., Willett, S., 1999. Spatial and temporal variations in exhumation of the central Swiss Alps and implications for exhumation mechanisms. In: Ring, U., Brandon, M.T., Lister, G.S., Willett S. (Eds.), Exhumation Processes: Normal Faulting , Ductile Flow and Erosion, Geol. Soc. London Spec. Publ. 154, pp. 157-179.

623 44. Tanaka, T., Togashi, S., Kamioka, H., Amakawa, H., Kagami, H., et al., 2000. JNdi-1: a
624 neodymium isotopic reference in consistency with La Jolla neodymium. Chem. Geol. 168,
625 279–281.

626 45. Valla, P. G., Shuster, D. L., van der Beek, P. A., 2011. Significant increase in relief of the
627 European Alps during mid-Pleistocene glaciations. Nat. Geosci. 4(10), 688-692.

628 46. Vezzoli, G., Garzanti, E., Limonta, M., Andò, S., Yang, S., 2016. Erosion patterns in the
629 Changjiang (Yangtze River) catchment revealed by bulk-sample versus single-mineral
630 provenance budgets. Geomorphology, 261, 177-192.

631 47. von Eynatten, H., Dunkl, I., 2012. Assessing the sediment factory: the role of single grain
632 analysis. Earth-Sci. Rev., 115(1), 97-120.

633 48. Wasserburg, G.J., Jacobsen, S.B., DePaolo, D.J., McCulloch, M.T., Wen, T., 1981. Precise
634 determination of Sm/Nd ratios, Sm and Nd isotopic abundances in standard solutions.
635 Geochim Cosmochim. Acta 45, 2311–2323.

636 49. Willett, S. D., 2010. Late Neogene erosion of the Alps: a climate driver?. Annu. Rev. Earth
637 Planet. Sci. 38, 411-437.

638 50. Wittmann, H., Malusà, M. G., Resentini, A., Garzanti, E., Niedermann, S., 2016. The
639 cosmogenic record of mountain erosion transmitted across a foreland basin: Source-to-sink
640 analysis of in situ ^{10}Be, ^{26}Al and ^{21}Ne in sediment of the Po river catchment. Earth Planet. Sci.
641 Lett. 452, 258-271.

642 51. Wobus, C. W., Whipple, K. X., Hodges, K. V., 2006. Neotectonics of the central Nepalese
643 Himalaya: Constraints from geomorphology, detrital ^{40}Ar/^{39}Ar thermochronology, and
644 thermal modeling. Tectonics 25(4).

645 52. Wu, F.Y., Yang, Y.H., Xie, L.W., Yang, J.H., Xu, P., 2006. Hf isotopic compositions of the
646 standard zircons and baddeleyites used in U/Pb geochronology. Chem. Geol. 234, 105–126.

647 53. Xie, L.W., Zhang, Y.B., Zhang, H.H., Sun, J.F., Wu, F.Y., 2008. In situ simultaneous
648 determination of trace elements, U–Pb and Lu–Hf isotopes in zircon and baddeleyite. Chinese
649 Sci. Bull. 53, 1565–1573.

650 54. Yang, Y.H., Sun, J.F., Xie, L.W., Fan, H.R.,Wu, F.Y., 2008. In situ Nd isotopic measurement
651 of geological samples by laser ablation. Chinese Sci. Bull. 53, 1062–1070.

652 55. Zanchetta, S., Malusà, M. G., Zanchi, A., 2015. Precollisional development and Cenozoic
653 evolution of the Southalpine retrobelt (European Alps). Lithosphere 7(6), 662-681.

654 56. Zattin, M., Andreucci, B., Thomson, S. N., Reiners, P. W., Talarico, F. M., 2012. New
655 constraints on the provenance of the ANDRILL AND-2A succession (western Ross Sea,
656 Antarctica) from apatite triple dating. Geochem. Geophys. Geosyst. 13 (10).

657 57. Zhao, L., Paul, A., Malusà, M. G., Xu, X., Zheng, T., Solarino, S., Guillot, S., Schwartz, S.,
658 Dumont, T., Salimbeni, S., Aubert, C., Pondrelli, S., Wang, Q., Zhu, R., 2016. Continuity of
659 the Alpine slab unraveled by high-resolution P-wave tomography. J. Geophys. Res.
660 doi:10.1002/2016JB013310.

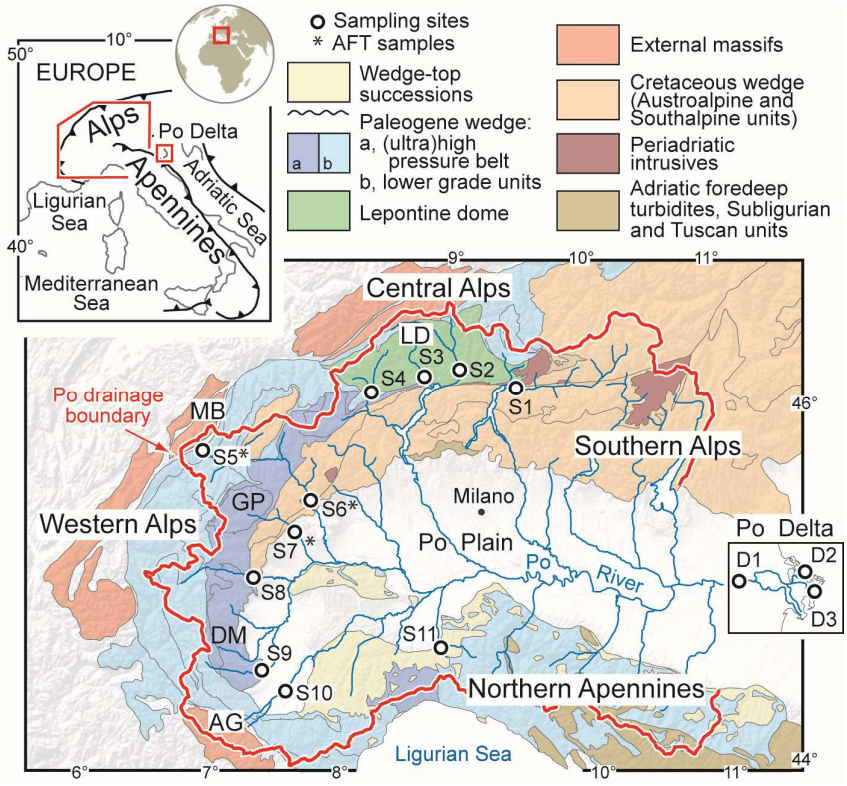

Fig. 1. Tectonic map of the European Alps and sample locations (S1-to-S11 and D1-to-D3). The red line indicates the boundary of the Po river catchment. Acronyms: AG, Argentera; DM, Dora-Maira; GP, Gran Paradiso; LD, Lepontine dome; MB, Mont Blanc (simplified after Malusà et al., 2015).

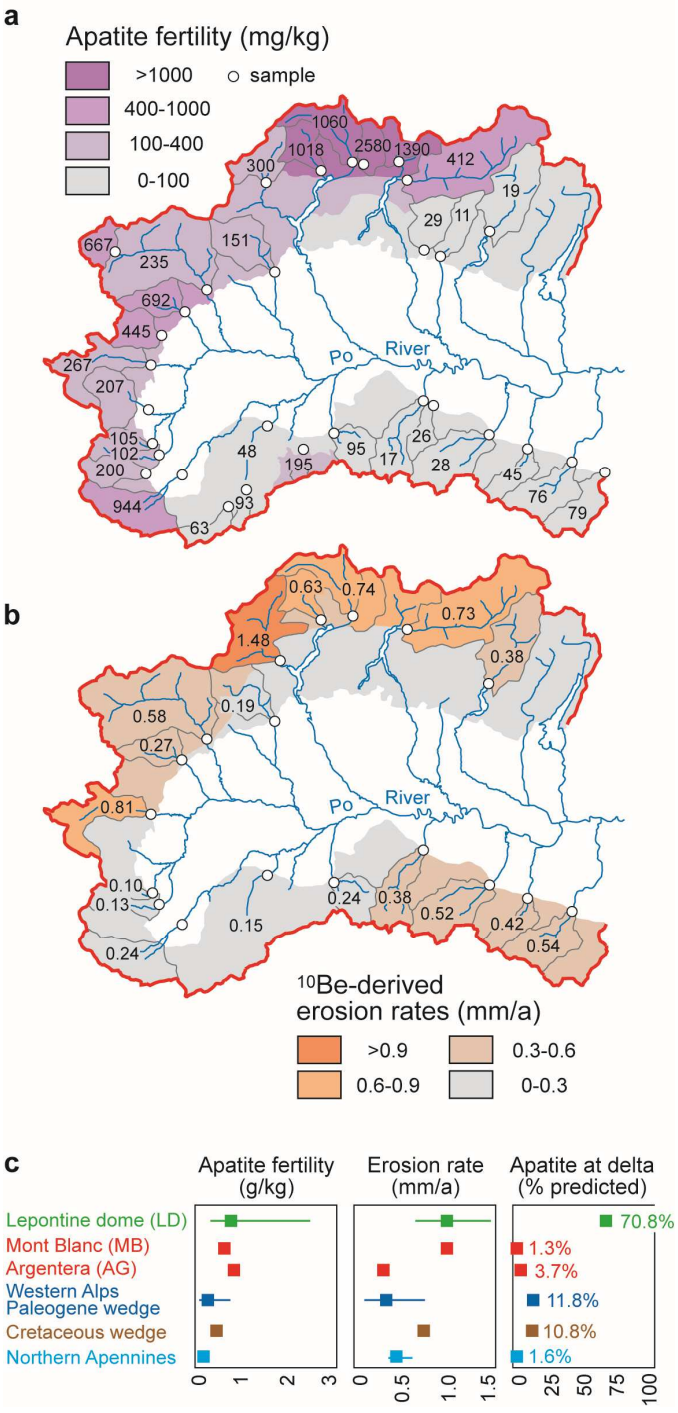

669

670 **Fig. 2.** Predicted apatite contribution to the Po delta based on apatite-fertility data and cosmonuclide-
671 derived erosion rates in the source areas. **a**, Apatite fertility map of the Po river catchment based on
672 mineral concentrations measured in modern river sand samples (white dots) (from Malusà et al., 2016a);
673 **b**, Erosion rates based on cosmogenic ^{10}Be concentrations in quartz grains from modern river sand
674 samples (white dots) (from Wittmann et al., 2016); **c**, Expected apatite contribution calculated for the
675 major sediment sources.

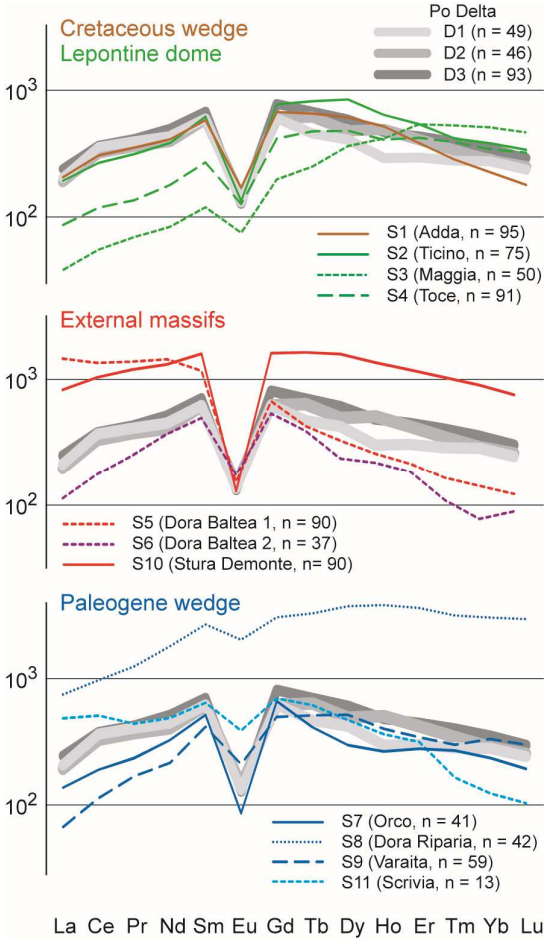

Fig. 3. Median values of chondrite-normalised trace-element patterns. The three Po delta samples (thick gray lines) show consistent patterns with MREE enrichment and a strong Eu anomaly; similar patterns are observed in samples S1, S2 and S7 (see supplementary Fig. S1 for single-grain spider diagrams).

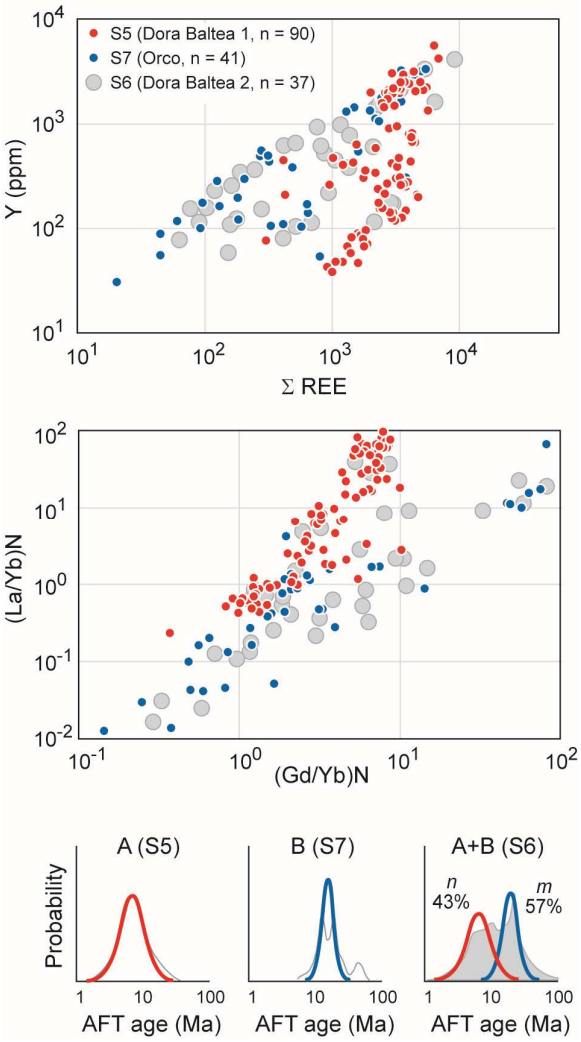

684

685

686

687 **Fig. 4.** Comparison between trace-element and fission-track data in detrital apatite from the northern
688 Western Alps. Trace-element diagrams (upper and intermediate panels) show that apatite grains shed
689 from the External Massifs (red dots) and from the metamorphic wedge (blue dots) are geochemically
690 distinct, and combined in a proportion 2:3 in sample S6 (large gray dots). The same proportion is
691 obtained from apatite fission-track data (AFT, lower panel).

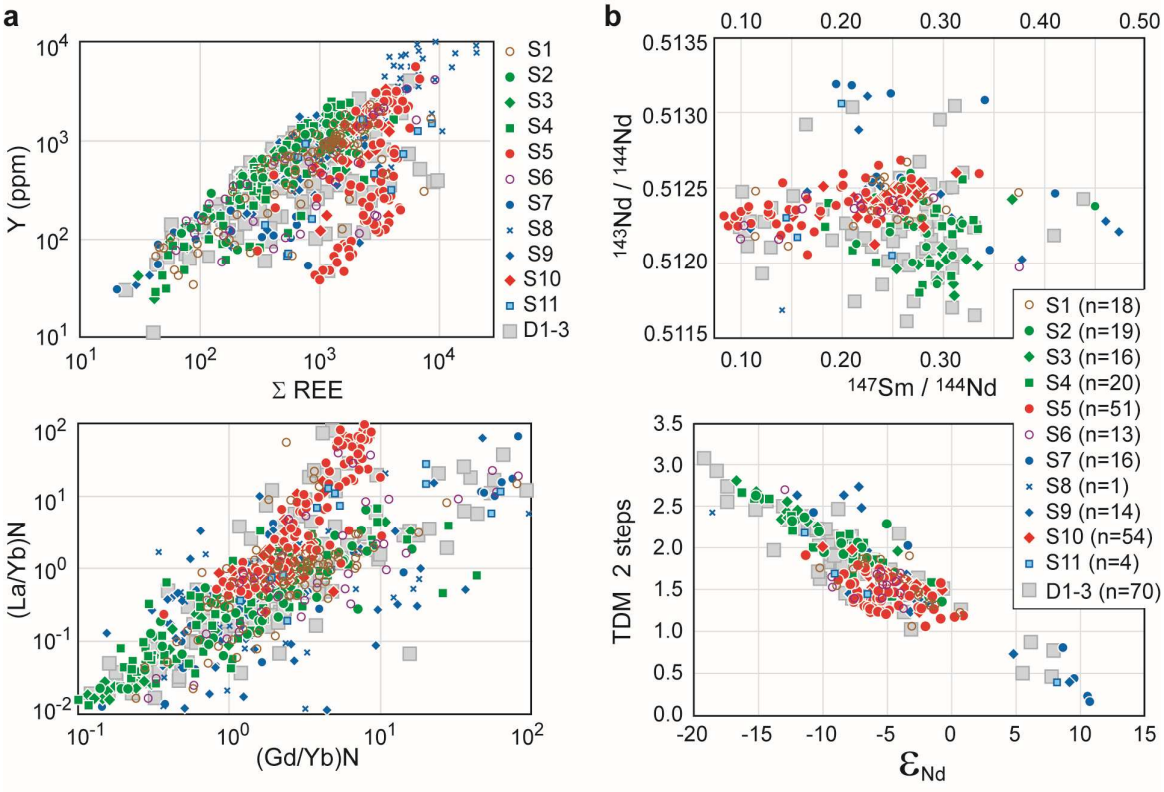

692
693
694
695

696 **Fig. 5.** **a,** Trace elements in detrital apatite from major Alpine rivers consistently match the
697 distribution observed in the Po delta (gray squares); apatite grains from the Lepontine dome (in green)
698 and the External Massifs (in red) are geochemically distinct; apatite grains on the top right of the
699 (La/Yb)N vs (Gd/Yb)N diagram are consistent exclusively with a Paleogene wedge source (in blue).
700 **b,** Nd isotopes effectively mirror the diverse tectonometamorphic evolution of eroded Alpine units;
701 model ages (TDM) in apatite from the External Massifs (in red) are in the range of 1 to 2 Ga, but may
702 reach values approaching 3 Ga in samples from the Lepontine area (in green), and are occasionally
703 <1 Ga in samples from the Paleogene wedge (in blue).

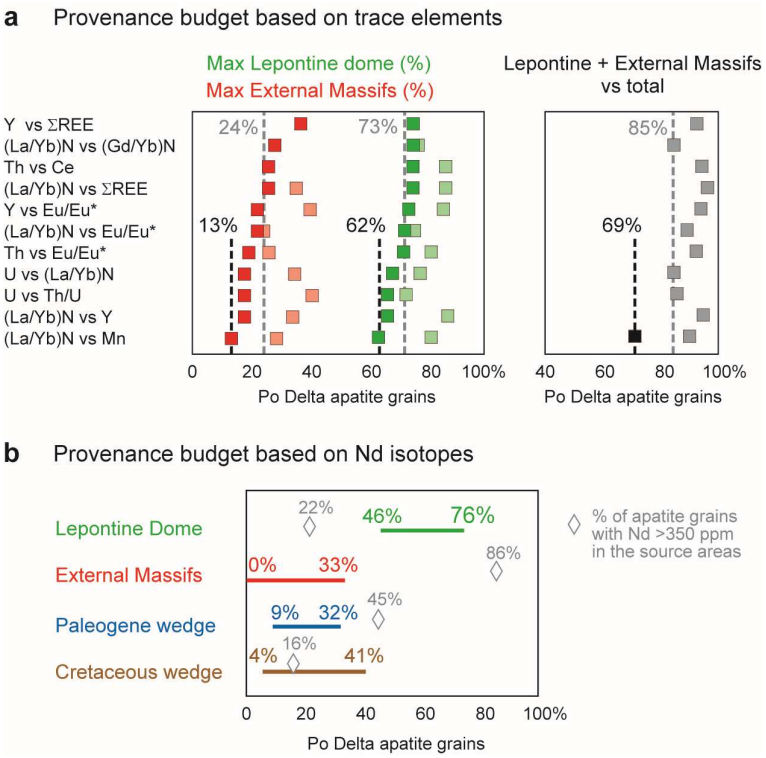

Fig. 6. **a,** Provenance budget based on the analysis of 11 different combinations of trace-element parameters, performed either separately (pale squares) or sequentially (dark squares). Apatite contribution cannot exceed 62% for the Lepontine dome, 13% for the External Massifs, and 69% in total for Lepontine + External Massif sources. Such values are higher (gray numbers) if discrimination diagrams are applied separately.

b, Provenance budget based on Nd-isotopic compositions: analyzed apatite grains derived from the Lepontine sources may range from a minimum of 46% to a maximum of 76%. This is a minimum estimate, because only 22% of all apatite grains from the Lepontine dome have Nd > 350 ppm, and are thus suitable for Nd isotopic measurements (gray lozenges). Provenance from the External Massifs (0-33%) is instead largely overestimated (86% apatite grains with Nd > 350 ppm).

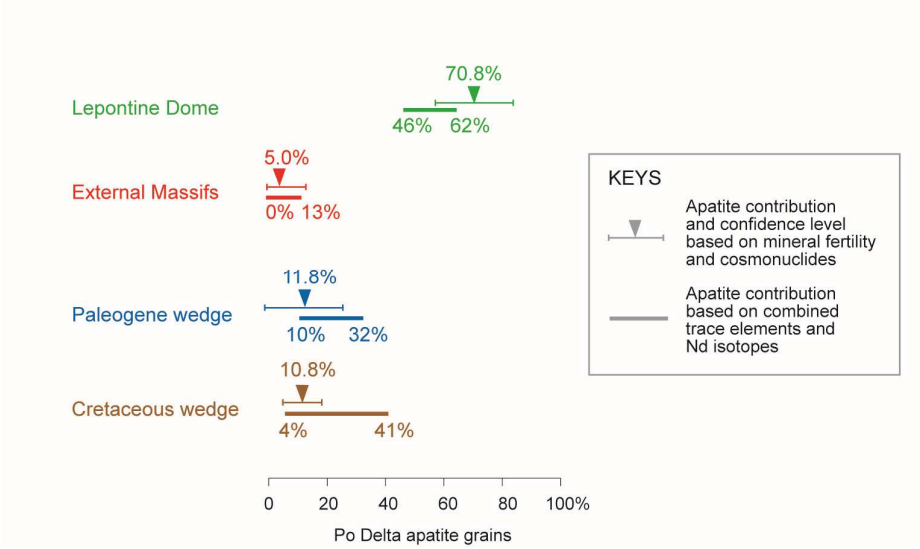

717

718

719

720 **Fig. 7.** Apatite contributions to the Po delta predicted from trace elements and Nd isotopes in detrital
721 apatite (representing 0.0002% to 0.25% weight of a sediment sample) are consistent with the range
722 independently derived from mineral fertility data and ^{10}Be analysis of quartz grains (representing ~30
723 to >50 weight % of the same sample). Error bars for predicted contributions encompass uncertainties
724 in ^{10}Be-derived erosion rates.

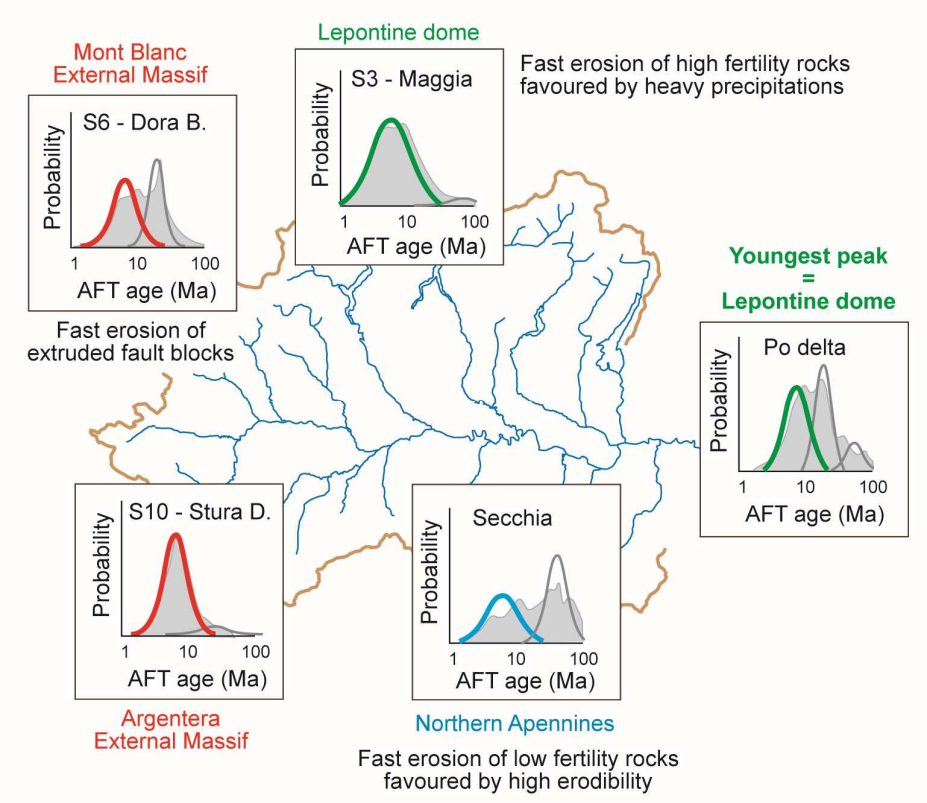

Fig. 8. Apatite fission-track (AFT) data from the Po delta, and representative grain-age distributions from the main detrital sources (i.e., the External Massifs, the Lepontine dome and the Northern Apennines) potentially contributing young apatite grains (AFT age <10 Ma) to the final sediment sink. Trace-element and Nd-isotope data point to an almost exclusive Lepontine origin for such young apatite grains (see Fig. 7), which implies that the detrital thermochronology record is largely controlled by high-fertility source rocks (AFT data from Malusà et al., 2009a; Garzanti et al., 2012; Malusà and Balestrieri, 2012; Resentini and Malusà, 2012).

Supplementary data:

Supplementary Table S1: Apatite provenance – predictions based on fertility and cosmonuclide data

Supplementary Table S2: Sample locations

Supplementary Table S3: Full trace-element dataset

Supplementary Table S4: Full Nd-isotope dataset

Supplementary Table S5: Provenance budgets based on trace-element data

Supplementary Fig. S1: Single-grain chondrite-normalised trace-element patterns

Supplementary Fig. S2: Full trace-element diagrams

Supplementary Fig. S3: Full discrimination diagrams based on trace-element data

Supplementary Fig. S4: Discrimination diagrams based on Nd isotopes

Supplementary Fig. S5: Apatite fission-track data